NOVEL BROADBAND DIRECTION OF ARRIVAL ESTIMATION USING LUNEBURG LENS

Graduate Students: Xiaoju Yu [(1)], Min Liang [(1)] and Rafael Sabory-Garcia[(1)]

Faculty Advisors: Michael Gehm [(1)] and Hao Xin* [(1)]

(1) Electrical and Computer Engineering Department, University of Arizona, Tucson, AZ 85721

ABSTRACT

A broadband passive direction finding system utilizing Luneburg lens has been investigated. With the simulated power level distribution at the detectors mounted on a Luneburg lens, both Cramér–Rao bound (CRB) and the root mean square error (RMS) based on the Correlation Algorithm (CA) for the direction of arrival (DoA) estimation have been derived and calculated. Guidelines on how to design the Luneburg lens detecting system have been studied. Finally, as a proof-of-concept demonstration, the DoA performance of a Luneburg lens fabricated using the polymer jetting technology with five detectors 10º equally spaced to receive the azimuth signal from -20º to 20º is demonstrated.

Key Words: Correlation Algorithm, Cramér–Rao Bound, Direction Finding, Luneburg Lens, Polymer Jetting

INTRODUCTION

Microwave passive direction finding is a very important technology that has many military and commercial applications including electronic warfare [1], mobile communications [2], etc. A typical microwave direction finding system may use an array consists of a large number of antenna elements and sophisticated algorithms to achieve high degree of accuracy [1]. However, the size, weight, and cost associated with the large number of hardware components and the complicated signal processing can be impractical. In [3], a lossy scatterer in between two monopoles direction finding system is proposed to reduce the system size and cost. However, all these systems are relatively narrow banded because of the intrinsic antenna element property. Luneburg lens [4] based direction finding system proposed in this paper is a good candidate to

achieve a low cost, accurate and broadband direction finding system.

A Luneburg lens has the characteristic that every point on the surface of the lens is the focal point of a plane wave incident from the opposite side as shown in Fig. 1. With a number of detectors mounted on the surface of a Luneburg lens, the DoA can be estimated by considering the received power distribution on all the detectors. This novel direction finding system is advantageous in that it is really wide banded and it does not require any expensive phase shifter component. In addition, the high gain property of a Luneburg lens leads to small correlation between received power distributions for different incident angles, thus high accuracy for the incident angle estimation can be achieved.

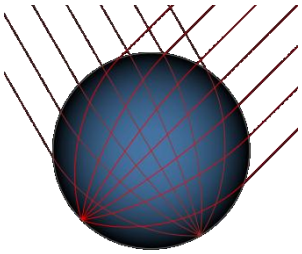

Figure1. Optical path of plane waves coming into a Luneburg lens.

In this paper, the Luneburg lens design is first studied. Next the Luneburg lens direction finding system is described. The performance of this system is investigated with the proposed correlation DoA estimation method. To quantitatively evaluate it, the RMS error of the proposed correlation method is compared with that of the Cramer Rao bound. Finally, as a proof-of-concept demonstration, a Luneburg lens is fabricated and measured with five detectors equally spaced by 10^o separation on the equator of the spherical lens. The corresponding DoA performance is reported with the azimuth incident signal from -20^o to 20^o.

LUNEBURG LENS DESIGN

A spherical Luneburg lens is a gradient index device which has a spatial dielectric constant distribution of $\varepsilon_r = 2 - (r/R)^2$ (r is distance from the center of the sphere and assuming the magnetic permeability of 1). The conventional methods for building a 3-D spherical Luneburg Lens are quite expensive and time consuming. Recently developed polymer-jetting rapid prototyping technique [5] has allowed 3-D Luneburg lens be fabricated easily and with much lower cost than traditional methods. The left picture in Fig. 2 shows the designed Luneburg lens structure of a radius R of 6cm. This gradient dielectric is realized by unit cells as shown in the right picture in Fig. 2. The unit cell consists of a center polymer cube with an ε_r of 2.7 and an outside air void. The effective permittivity of the unit cell is controlled by the filling ratio (dependent on the cube dimension b as labeled in Fig. 2) between the polymer and the air void.

The antenna gains of the Luneburg lens for frequency from 8.2GHz~12.4GHz (because of large time consuming of this simulation, not all frequencies in the range are analyzed) are simulated and plotted in Fig. 3. It can be seen that the gain is quite high, about 20dB for all frequencies. As frequency goes higher, the gain increases and the half power beam width (HPBW) decreases as expected.

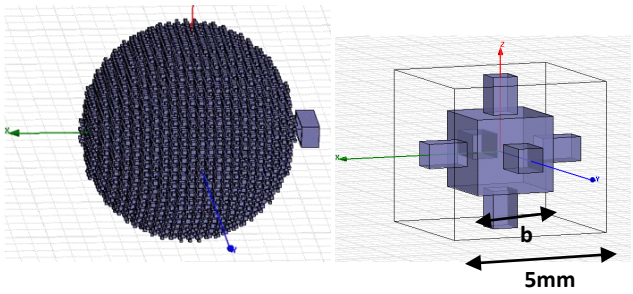

Figure 2. HFSS model of the Luneburg lens (left) and a unit cell of the lens (right).

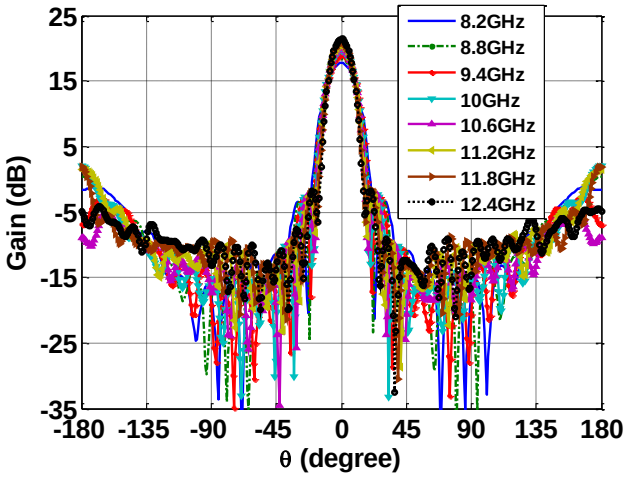

Figure 3. The Luneburg lens antenna gain patterns (simulation results) at different frequencies with θ from -180° to 180° (1° step).

LUNEBURG LENS DIRECTION FINDING PERFORMANCE ANALYSIS

As shown in Fig. 4, a 6cm-radius Luneburg lens with several equally spaced detectors mounted on the surface is proposed as the broadband direction finding model.

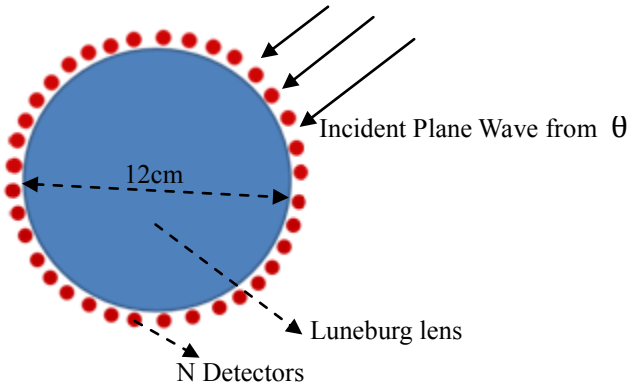

Figure 4. Schematic of the Luneburg lens direction finding system.

Correlation algorithm (CA) is applied for the azimuth DoA estimation. For $\forall$ incident θ, the cross-correlation coefficients are first calculated:

$$\rho(\theta_m) = \mathrm{Corr}\big(y(\theta), x(\theta_m)\big),\ m=1, 2\ldots M \quad (1),$$

where M is the number of incident angles, $y = (y_1, y_2, y_3 \ldots y_N)$ is the received power level distribution at N detectors; $x = (x_1, x_2, x_3 \ldots x_N)$ is the pre-saved power level distribution without noise as the calibration set of data. Then the angle with peak correlation coefficient is estimated as the incident angle:

$$\hat{\theta} = \arg\ \max_{\theta}\{\rho(\theta_1), \rho(\theta_2) \ldots \rho(\theta_M)\} \quad (2).$$

To quantitatively evaluate the performance of the proposed Luneburg lens detecting system, the Cramér–Rao bound (CRB - a lower bound on the variance of any unbiased estimator) [6][7] of the DoA estimation error is also derived. The CRB for a single variable θ is:

$$\mathrm{Var}(\hat{\theta}) \geq 1/\mathrm{E}[\tfrac{\partial \ln f(y|\theta)}{\partial \theta}]^2 \quad (3).$$

Assume the received power level at detector #n (y_n) is obtained under a background of white Gaussian noise ~ N (0, σ^2), the CRB can be derived as (4)-(6):

$$f(y_n|\theta) = \tfrac{1}{\sqrt{2\pi}\sigma} \exp\{-\big(y_n - x_n(\theta)\big)^2/2\sigma^2\} \quad (4),$$

$$\mathrm{E}[\tfrac{\partial \ln f(y|\theta)}{\partial \theta}]^2 = \tfrac{1}{\sigma^2}\sum(\partial x_n/\partial\theta)^2 \quad (5),$$

$$\sigma(\hat{\theta})_{\mathrm{CRB}} = \sqrt{\sigma^2/\sum(\partial x_n/\partial\theta)^2} \quad (6),$$

where $\sigma(\hat{\theta})_{\mathrm{CRB}}$ is the CRB for the RMS error of θ.

Figure 5 shows the calculated RMS error vs. incident angle θ at 10GHz when 36 detectors in total are uniformly placed on the surface of the lens (10° angle interval) and the signal to noise ratio (SNR) equals to 15dB. The SNR is defined as the received power over the added Gaussian white noise level at the detector where the incoming wave is from the opposite side of the lens. The calculated CRB of the RMS error is lower than 1.8° and periodic with incident angle (the period is the same as the angle spacing of the detectors ~10° as expected). Because of the periodicity, the RMS error versus incident angle only from -45° to 45° is shown in Fig.5 instead of the full 360° range. The RMS error based on the correlation method (1000 runs) is larger as expected but really close to the CRB, indicating a good estimation of this method under high SNR. The sharp peak of the RMS error based on correlation method around 25° is due to non-ideal Gaussian white noise model in the matlab software.

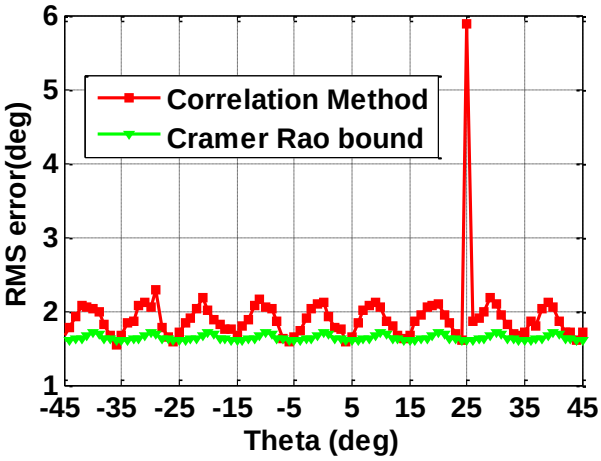

Figure 5. RMS error vs. incident angle (SNR=15dB and frequency at 10GHz) with received power from 36 detectors obtained from simulation.

The DoA performance of the Luneburg lens system under different SNR level is also studied. Figure 6 demonstrates the RMS error vs. SNR (averaged over all angles from -180° to 180°) with 36 detectors at 10GHz. The RMS error increases with lower SNR. For SNR > 15dB, the calculated RMS error with the correlation method is almost the same as the CRB (less than 2°) while for SNR<15dB, it increases sharply with further reduced SNR. It is concluded from Fig. 5 that the correlation method performs well for high SNR environment and crashes down under too noisy background.

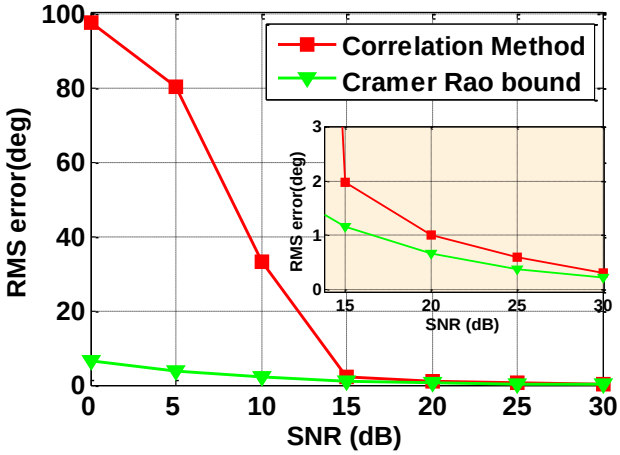

Figure 6. RMS error vs. SNR (averaged over all angles -180° ~ 180°) with 36 detectors at 10GHz.

In addition, the impact of different number of detectors on the DoA performance of the Luneburg lens system is analyzed. As shown in Fig. 7, the CRB increases slowly with decreasing number of detectors first and then increases rapidly. The number of detectors of the turning point is about 24. For all cases, the CRB for the RMS error is lower than 6° for SNR=15dB and frequency from

8.2GHz to 12.4GHz.

As a comparison, the RMS error of the correlation method vs. the number of detectors at different frequencies is plotted in Fig. 8. The RMS error of the correlation method is close to the CRB for number of detectors > 30 and much higher for small number of detectors. Figure 8 also shows a smaller estimation error for lower frequency which is due to larger average received power level at all the detectors (wider HPBW for lower frequency).

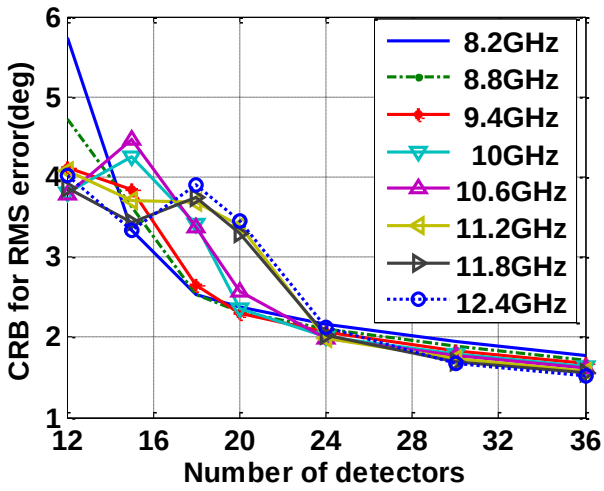

Figure 7. CRB vs. number of detectors (averaged over all angles -180° ~ 180°) with SNR=15dB.

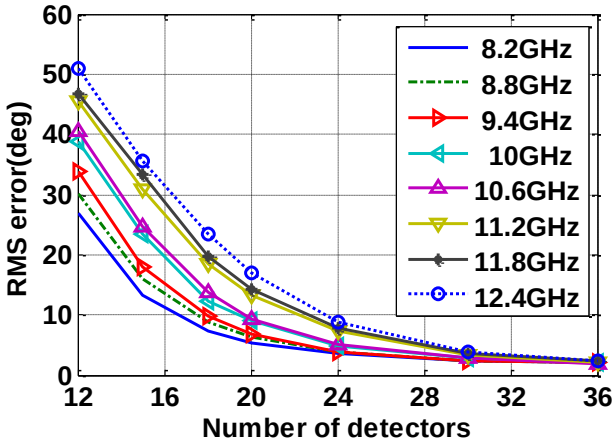

Figure 8. RMS error of the correlation method vs. number of detectors (averaged over all angles from -180° to 180°) with SNR=15dB (1000 runs).

It is found that in an additive Gaussian white noise environment, the CA performs better for higher SNR and larger number of detectors as expected. The simulated DoA estimation accuracy can reach 2º for SNR = 15dB and frequency range within 8.2 - 12.4GHz. Guidelines on how to design the Luneburg lens detecting system under certain noise environment and frequency range of interest has been provided.

MEASUREMENT RESULTS

As a proof-of-concept experimental demonstration, a Luneburg lens (as shown in Fig. 9) fabricated using the polymer jetting technology with a radius of 12cm (finite-element simulation of this-large lens in HFSS is currently not practical) is measured. Although the Luneburg lens used is broadband (at least from 3 – 12 GHz), without losing generality, an operating frequency of 5.6 GHz is selected at which the detectors have its peak sensitivity. In the experiment, a signal generator (Agilent E8257C) connected to a double ridged horn antenna is used as the transmitting source. A picture of the experiment setup for the direction finding is shown in Fig. 9. Five detectors with a separation of 10 degrees are mounted on the surface of the lens in our initial tests. The distances from the transmitting horn to the Luneburg lens are 3 m and 4 m, for the calibration and the performance test, respectively (both in the far-field). The detector is made of a zero biased diode (SMS7630-061) fed by a monopole antenna printed on an 8-mil Duroid-RO4003C substrate.

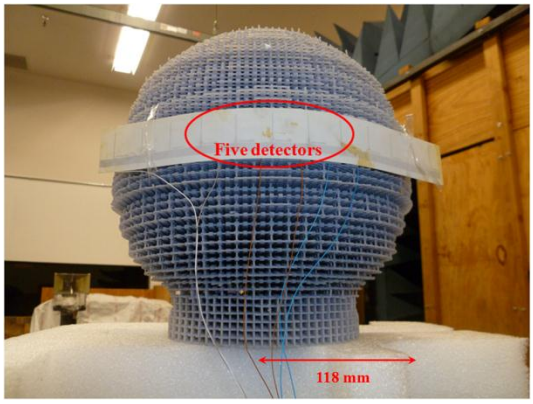

Figure 9. Experimental setup of a Luneburg lens with 5 detectors mounted.

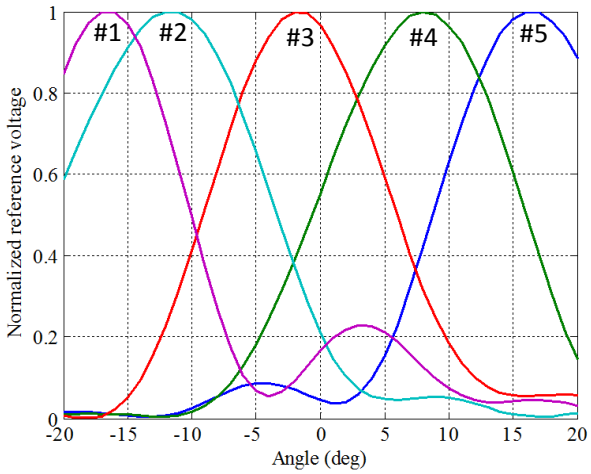

Figure 10. Normalized detectors' (#1, #2, #3, #4, #5) output voltages as the calibration (the Luneburg lens is 3 meters away from the source).

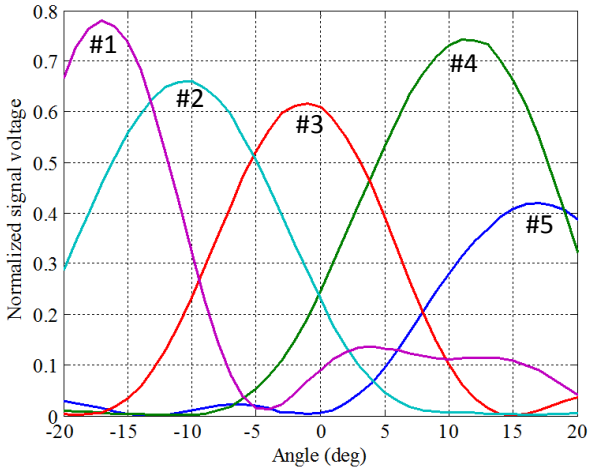

Figure 11. Normalized detectors' (#1, #2, #3, #4, #5) output voltages in DF test (the Luneburg lens is 4 meters away from the source).

The output voltages of all the 5 detectors are recorded with different incident angles from -20° to 20°. All the voltages are normalized to the peak values when they are directly facing the source in the calibration. Figures 10 and 11 plot the normalized voltages on each detector of the calibration and test measurements, respectively. The reason for the peak values of different detectors being different in Fig. 11 is that the sensitivity of each detector is different at different power levels (the output voltages of some detectors decrease faster than others with decreasing power).

The correlation algorithm discussed in the previous section is applied to estimate the source direction. For each testing incident angle, the normalized signal data in Fig. 11 was correlated to the normalized calibration data from all the directions. The angle with peak correlation is the estimated direction of the incident wave.

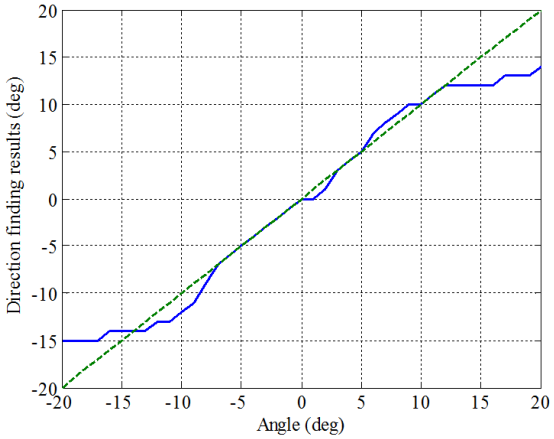

Figure 12. Estimated direction results at different incident angles from -20° to 20°.

Figure 12 plots the estimated direction with the proposed Luneburg lens system versus the actual

incident angle. The estimation error of the CA method with the 5-detector Luneburg lens system is smaller than 2^o for incident angles from -15^o to 15^o, and it degrades to about 5^o for incident angles up to -20^o and 20^o. The larger error for incident angles beyond +/- 15^o is due to the limited number of detectors in the experiment. For example, beyond +/- 15^o, the 5-detectors system starts to lose its coverage. With a Luneburg lens direction finding system with fully populated detectors (i.e., 36 detectors with 10^o separation), accurate DOA in the entire azimuth plane should be obtained. If detectors are populated in a 3-D fashion on the lens surface, accurate 3-D direction finding can be obtained.

CONCLUSION

In this paper, a broadband passive direction finding system utilizing Luneburg lens has been investigated. A number of detectors are mounted around the surface of the lens to estimate the direction of arrival (DOA) of a microwave signal utilizing the received power distribution of the detectors. It is found that in an additive Gaussian white noise environment, the CA performs better under higher signal to noise ratio (SNR) and larger number of detectors, as expected. The simulated DoA estimation accuracy can reach 2º for SNR = 15dB and within frequency range from 8.2GHz to 12.4GHz. Guidelines on how to design the Luneburg lens detecting system has been studied and provided. As a proof-of-concept demonstration, a Luneburg lens fabricated using the polymer jetting technology with five detectors 10º equally spaced is measured at 5.6 GHz. The DoA estimation results using the CA show that the estimated error is smaller than 2º within -15º to 15º incident angles.

ACKNOWLEDGEMENT

This work was supported in part by the U.S. Army Research Laboratory and the U.S. Army Research Office under agreement number W911NF-1-01-0285 and by the National Science Foundation under Awards 0823864 and 0925220.

REFERENCES

[1] S. E. Lipsky, Microwave Passive Direction Finding, John Wiley & Sons, Inc., New York, 1987.

[2] L.C. Godara, "Application of antenna arrays to mobile communications. II. Beam-forming and direction-of-arrival considerations," Proc. IEEE, Vol. 85, no. 8, pp. 1195-1245, 1997.

[3] R. Zhou, H. Zhang and H. Xin, "Improved Two-Antenna Direction Finding Inspired by Human Ears," IEEE Trans. on Antennas and Propagation, Vol. 59, No. 7, 2011.

[4] R. K. Luneburg, Mathematical Theory of Optics., Los Angeles, CA: Univ. California Press, 1964.

[5] M. Liang, W. Ng, K. Chang, M. Gehm, H. Xin, “An X-Band Luneburg Lens Antenna Fabricated by Rapid Prototyping Technology,” IEEE International Microwave symposium, June, 2011

[6] Cramér, Harald, Mathematical Methods of Statistics, Princeton, NJ: Princeton Univ. Press., 1946.

[7] Rao, Calyampudi Radakrishna, "Information and the accuracy attainable in the estimation of statistical parameters". Bulletin of the Calcutta Mathematical Society, 1945.